Supporting Information for

Deciphering the selectivity descriptors of heterogeneous metal phthalocyanine electrocatalysts for hydrogen peroxide production

Yubo Yuan, Huan Li, Zhan Jiang, Zhichao Lin, Yirong Tang, Hongxuan Wang, Yongye Liang*

Department of Materials Science and Engineering, Southern University of Science and Technology, Shenzhen 518055, China.

* Corresponding Author: Y. Liang: liangyy@sustech.edu.cn

Contents

Supporting Methods

Chemicals and materials

Zinc phthalocyanine (ZnPc, GR, ACROS), copper phthalocyanine (CuPc, ≥95%, Alfa Aesar), manganese phthalocyanine (MnPc, 100%, Alfa Aesar), cobalt phthalocyanine (CoPc, ≤100%, Alfa Aesar), nickel phthalocyanine (NiPc, 95%, Alfa Aesar), *N*,*N*-dimethyl formamide (DMF, 99.5%, Aladdin), ethanol (AR, Aladdin), sulfuric acid (H_2SO_4, AR, Guoyao), potassium hydroxide (KOH, 90%, Aladdin), potassium permanganate ($KMnO_4$, 99%), and polytetrafluoroethylene aqueous solution (PTFE, 60%, Aldrich) were used without further purification. Multiwalled carbon nanotubes (CNTs, FT-9100, C-Nano) were purified by the previous method.[1] Deionized water (18.2 MΩ·cm) was used in catalyst synthesis and electrochemical measurements. O_2 (99.9%) and Ar (99.999%) were purchased from Huashidai Gas Co. Ltd.

Synthesis of MPc MDEs

MPc MDEs (M = Co, Cu, Ni, Zn, Mn) were synthesized based on a reported approach.[2] In brief, purified CNTs (30 mg) were dispersed in DMF (30 mL) with the assistance of ultrasonication for 1 h. Meanwhile, a certain amount of MPc was dispersed in a small amount of DMF with the assistance of ultrasonication for 0.5 h. The two DMF suspensions were mixed in a round bottom flask with the assistance of ultrasonication for 0.5 h. Afterward, the round bottom flask was stirred at room temperature for 20 h. The precipitate was obtained by centrifugation and washed with DMF (3 times), ethanol (2 times), and water (1 time). Finally, the purified precipitates

were lyophilized to obtain MPc MDEs.

Material characterizations

Inductively coupled plasma mass spectrometry (ICP-MS) was performed on an Agilent Technologies 7700 series instrument. Transmission electron microscope (TEM) was performed on Titan ETEM. Atomic-resolution high-angle annular dark-field scanning transmission electron microscopy (HAADF-STEM) was performed on a double Cs-corrected FEI Themis G2 microscope. Energy-dispersive X-ray spectroscopy (EDS) elemental mappings was performed on a FEI Talos F200X. Scaning electron microscopy (SEM) was performed on a TESCAN MIRA3 LM model. Ultraviolet-visible (UV-Vis) absorption measurements were carried out with a Shimadzu UV-3600 spectrophotometer. The contact angle measurements of 29BC carbon paper and catalytic layers were performed on a goniometer (Optima, AST).

Electrochemical measurements

The fundamental electrochemical ORR and hydrogen peroxide reduction reaction (H_2O_2RR) performances were evaluated by a potentiostat (CH Instruments Ins., CHI 760E) in a standard three-electrode configuration electrochemical cell. Rotating ring-disk electrodes (RRDEs) with the disk area of 0.238 cm^2 and rotating disk electrodes (RDEs) with the disk area of 0.196 cm^2 were polished by alumina powder and were cleaned by deionized water and ethanol before electrochemical measurements. Then they were dried with high-purity Ar gas for standby. The electrocatalysts (1 mg) were

homogeneously dispersed in ethanol (130 μL) with Nafion (120 μL, 0.25 wt%) to form catalyst inks. For the catalyst inks of MPc + CNT, MPc (2 mg) and purified multi-walled CNTs (0.5 mg) were mixed directly in ethanol (325 μL) with Nafion (300 μL, 0.25 wt%). Then the catalyst inks were pipetted onto the disk of RRDEs and RDEs with the catalyst loading of 0.2 $mg \cdot cm^{-2}$ as working electrodes. The counter electrode was a graphite rod and the reference electrode was a saturated calomel electrode (SCE). The RRDEs and RDEs were rotated at a speed of 1600 rpm. Linear sweep voltammetry (LSV) for both ORR and H_2O_2RR experiments was performed with the scan rate of 5 mV s^{-1}, and the background current collected in an Ar saturated 0.1 M KOH electrolyte was deducted. For ORR measurements tested in O_2 saturated 0.1 M KOH electrolytes, the Pt rings of RRDEs were kept at 1.5 V versus reversible hydrogen electrode (RHE). The $2e^-$ ORR selectivity was calculated based on the following equation:

$$\text{Selectivity}\ (\%) = 200\% \times \frac{I_\text{R}/\text{N}}{I_\text{D} + I_\text{R}/\text{N}}$$

where I_R is the ring electrode current (A), I_D is the disk electrode current (A), and N is the ring electrode collection efficiency (0.29), which is calibrated by the redox of potassium ferricyanide (Figure S9). H_2O_2RR measurements were tested in Ar saturated 0.1 M KOH electrolytes containing 1 mM H_2O_2.

The kinetic current (I_K) was calculated from the following equation:

$$\frac{1}{I} = \frac{1}{I_\text{K}} + \frac{1}{I_\text{L}}$$

where I is the measured disk current (A) and I_L is the diffusion-limiting current (A). The $2e^-$ mass activity is calculated by the following equation:

$$2e^- \text{ mass activity}\ (\text{A/g}) = \frac{\text{FE}(H_2O_2) \times I_\text{K}}{m}$$

where H_2O_2 Faradaic efficiency ($FE(H_2O_2)$) was converted from corresponding selectivity at the same potential,[3] and m is the mass loading of catalysts on the working electrodes (g). The error bar of $2e^-$ mass activity represents the standard deviation of three independent samples.

The practical H_2O_2 electrosynthesis was further evaluated by homemade gas diffusion electrodes (GDEs). The catalyst inks contained with PTFE were prepared by dispersing the electrocatalysts (2 mg) in ethanol (850 μL), PTFE (100 μL, 1 wt%) and Nafion (50 μL, 0.5 wt%). And the catalyst ink without PTFE was prepared by dispersing the electrocatalysts (2 mg) in ethanol (950 μL) and Nafion (50 μL, 0.5 wt%). Working electrodes were prepared by drop-drying catalyst inks with the loading of 0.2 mg cm^{-2} on carbon papers (29BC, Sigracet). Then the electrodes were heated at 330 °C for 1 h under Ar to remove the surfactant in the PTFE solution. The frontside of working electrodes that exposing to cathode chamber was a round-shaped active area (0.5 cm^2) At the backside of the working electrodes, O_2 gas flow was purged into the gas chamber at 40 sccm. The catholyte and anolyte were both 1 M KOH, separated by a proton exchange membrane (Nafion 117). Fresh 1 M KOH were continuously injected into a small cathode chamber with the flow rate of 1 mL min^{-1} by a peristaltic pump to take the produced H_2O_2 out immediately. A Hg/HgO reference electrode was applied in this strongly alkaline environment. The concentration of generated H_2O_2 was evaluated every hour by using $KMnO_4$ titration. Specifically, the produced H_2O_2 in 1 mL electrolyte was collected at the cathode outlet and neutralized with excessive 0.5 M H_2SO_4, which was further quantified twice by 5 mM $KMnO_4$ solution. The average

amount of titrated $KMnO_4$ solution was recorded to calculate the amount of produced H_2O_2. Then the $\mathrm{FE}(\mathrm{H_2O_2})$ was calculated by the following equation:

$$\mathrm{FE}(\mathrm{H_2O_2})(\%) = \frac{2 \times 96485 \times R \times \mathrm{C}(\mathrm{H_2O_2})}{I} \times 100\%$$

where $\mathrm{C}(\mathrm{H_2O_2})$ is the concentration of produced H_2O_2 (M), I is the reduction current (A), and R is the flow rate of electrolyte (L s^{-1}). The production rate of H_2O_2 was calculated by the following equation:

$$\text{Production rate} = \frac{\mathrm{n}(\mathrm{H_2O_2})}{m \times t}$$

where $\mathrm{n}(\mathrm{H_2O_2})$ is the amount of produced H_2O_2 (mmol) and t is the measured time (h). The *iR* compensation was conducted after the electrochemical measurements. The cathodic energy efficiency was calculated according to the following equation:

$$\text{Cathodic energy efficiency} = \frac{\mathrm{FE}(\mathrm{H_2O_2}) \times E_{\mathrm{cell}}}{1.23 - V}$$

where E_{cell} is the thermodynamic cell potential (V) ($E_{\mathrm{cell}} = 0.47$ V for the $2e^-$ ORR pathway in alkaline media) and V is the applied potential versus RHE (V) after *iR* compensation.

The electrode potentials were all converted to versus RHE according to the following equation:

$$E_{\mathrm{RHE}} = E^{\mathrm{o}}_{\mathrm{ref}} + E_{\mathrm{ref}} + 0.0591 \times \mathrm{pH}$$

where the $E^{\mathrm{o}}_{\mathrm{SCE}}$ (saturated KCl) is 0.241 V or $E^{\mathrm{o}}_{\mathrm{Hg/HgO}}$ (1 M KOH) is 0.098 V at room temperature depending on the type of reference electrodes. The E_{ref} is measured working potential corresponding to reference electrodes.

UV-Vis Characterization

The structural stability of MPc after two-hour chronoamperometric measurement was proved by UV-Vis measurements. Briefly, UV-Vis absorption spectrum of CoPc was taken using its 0.05 mg mL^{-1} DMF solutions. The physically mixed CoPc+CNT was used for two-hour chronoamperometric measurement at 0.6 V since the CoPc content in physically mixed CoPc+CNT is much higher than CoPc MDE. The electrode was taken out from the electrolyte and quickly dipped into a vial containing 3 mL of deoxygenated DMF. The vial was gently sonicated for 10 s and then kept still for overnight, after which the supernatant was used for UV-Vis measurement.

Computational Methods

The first-principle calculation was based on the spin-polarized density functional theory (DFT) calculations by using the Vienna Ab Initio Simulation Package (VASP).[4] The generalized gradient approximation (GGA) in the form of Perdew-Burke-Ernzerhof (PBE) was used for the exchange-correlation potentials.[5-6] The projector augmented wave (PAW) pseudopotential was used for the core electrons.[7] The cutoff energy was 500 eV for the valence electrons. The convergence criteria for electronic relaxation and ionic relaxation to be 10^{-5} eV and 10^{-4} eV $Å^{-1}$, respectively. The cluster models were chosen and every MPc molecule was placed in a box in the size of 24×24×15 Å. The RMM-DIIS algorithm and Gamma-point-only grid were used for all the calculations. Grimme's DFT-D3 method was incorporated to implement the van der Waals correction.[8] The computational hydrogen electrode model was used to calculate the free energy profiles.[9] The free energy for each adsorbate was calculated by:

$$G = E + G_{\mathrm{correct}} + E_{\mathrm{sol}}$$

where E is the electronic energy by DFT, G_{correct} is the thermal correction to the free energy that was calculated by VASPKIT tool at 298.1 K.[10] E_{sol} is solvent correction where the implicit solvent model was applied by using VASPsol.[11-12] Within this model, the relative permittivity (ε_r) was set to be 2 and 5 for hydrophobic environment and 78.4 for bulk water.[13]

Since no contiguous active sites exist in MPc molecules, the dissociative pathway of O_2 is not possible to happen. The reaction pathways for ORR are listed below (* stands for the active site):

$$* + O_2 \rightarrow * O_2$$

$$* O_2 + H^+ + e^- \rightarrow * OOH$$

$$* OOH + H^+ + e^- \rightarrow * + H_2O_2 \quad \text{(Associative } 2e^- \text{ pathway)}$$

$$* OOH + H^+ + e^- \rightarrow * O + H_2O$$

$$* O + H^+ + e^- \rightarrow * OH$$

$$* OH + H^+ + e^- \rightarrow * + H_2O \quad \text{(Associative } 4e^- \text{ pathway)}$$

The produced H_2O_2 could be further adsorbed on MPcs and reduced to water (2+2e^- pathway), which is shown below:

$$* + H_2O_2 \rightarrow * H_2O_2$$

$$* H_2O_2 + H^+ + e^- \rightarrow * OH + H_2O$$

$$* OH + H^+ + e^- \rightarrow * + H_2O \qquad (2+2e^- \text{ pathway})$$

The absolute value of energy difference between 2.12 eV and the binding energy of *OOH at 0.7 V is the overpotential (U_O) of $2e^-$ pathway. The limiting potential (U_L)

of $2e^-$ pathway can be calculated according to the following equation:

$$U_L = 0.7 - U_O$$

Supporting Figures

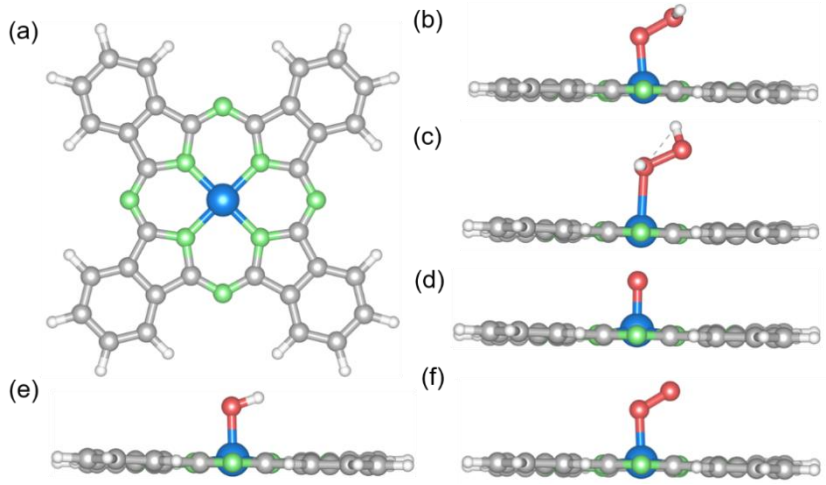

Figure S1. (a) Optimized configuration of CoPc. And the most stable configurations of (b) *OOH, (c) *H_2O_2, (d) *O, (e) *OH, and (f) *O_2 on CoPc.

Note: The sample calculation of CoPc for the free energy changes during oxygen reduction elementary steps is given. The electronic energy of each intermediate is listed below:

Intermediate	*	*OOH	*O	*OH	*H_2O_2	*O_2
E (eV)	-423.77	-438.24	-428.30	-433.69	-442.25	-434.20

And the vibrational frequencies for each absorbate are listed below:

Intermediate	Vibrational frequencies (cm^{-1})
*OOH	3593.55, 1293.08, 888.98, 499.41, 396.96, 246.59, 117.55, 98.55 42.59
*O	669.62, 166.21, 161.46
*OH	3686.14, 944.60, 522.57, 162.11, 155.85, 87.41
*H_2O_2	3656.61, 3630.51, 1339.79, 1230.50, 810.54, 516.69, 222.71, 172.81, 115.69, 66.16, 54.29, 26.80

We further used the VASPKIT code for post-processing of the VASP calculated data. According to VASPKIT, the vibrational frequencies less than 50 cm^{-1} were set to

50 cm^{-1} to avoid abnormal entropy contribution. And the PV contribution was neglected. The G_{correct} was calculated by:

$$G_{\mathrm{correct}} = \mathrm{ZPE} + \Delta U(\mathrm{T}) - TS$$

where ZPE is the zero-point energy, $\Delta U(\mathrm{T})$ is the change of internal energy from 0 K to room temperature, and *TS* is the entropy contribution.

The entropy *S* is listed below:

Intermediate	*OOH	*O	*OH	*H_2O_2
S (meV/K)	0.651	0.232	0.253	0.959

The G_{correct} is listed below:

Intermediate	*OOH	*O	*OH	*H_2O_2
$\boldsymbol{G}_{\mathrm{correct}}$ (eV)	0.34	0.03	0.30	0.57

Then we directly applied the widely used VASPsol software to calculate E_{sol} as following:

Intermediate	*	*OOH	*O	*OH	*H_2O_2
$\boldsymbol{E}_{\mathrm{sol}}$ (eV)	-0.58	-0.79	-0.73	-0.75	-0.93

The free energy for each adsorbate of CoPc was calculated by:

$$G = E + G_{\mathrm{correct}} + E_{\mathrm{sol}}$$

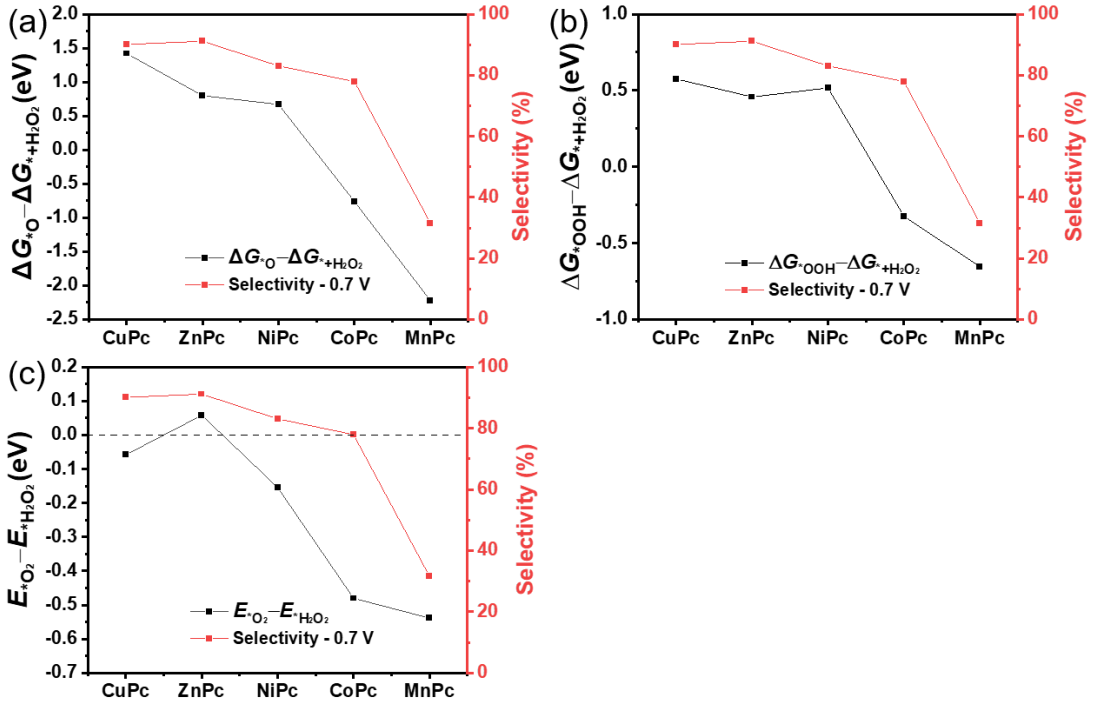

Figure S2. Correlation between other possible descriptors (a) $\Delta G_{*\mathrm{O}} - \Delta G_{*+\mathrm{H_2O_2}}$, (b) $\Delta G_{*\mathrm{OOH}} - \Delta G_{*+\mathrm{H_2O_2}}$, previously reported descriptor (c) $E_{*\mathrm{O_2}} - E_{*\mathrm{H_2O_2}}$[14] and measured selectivities of MPc MDEs at 0.7 V.

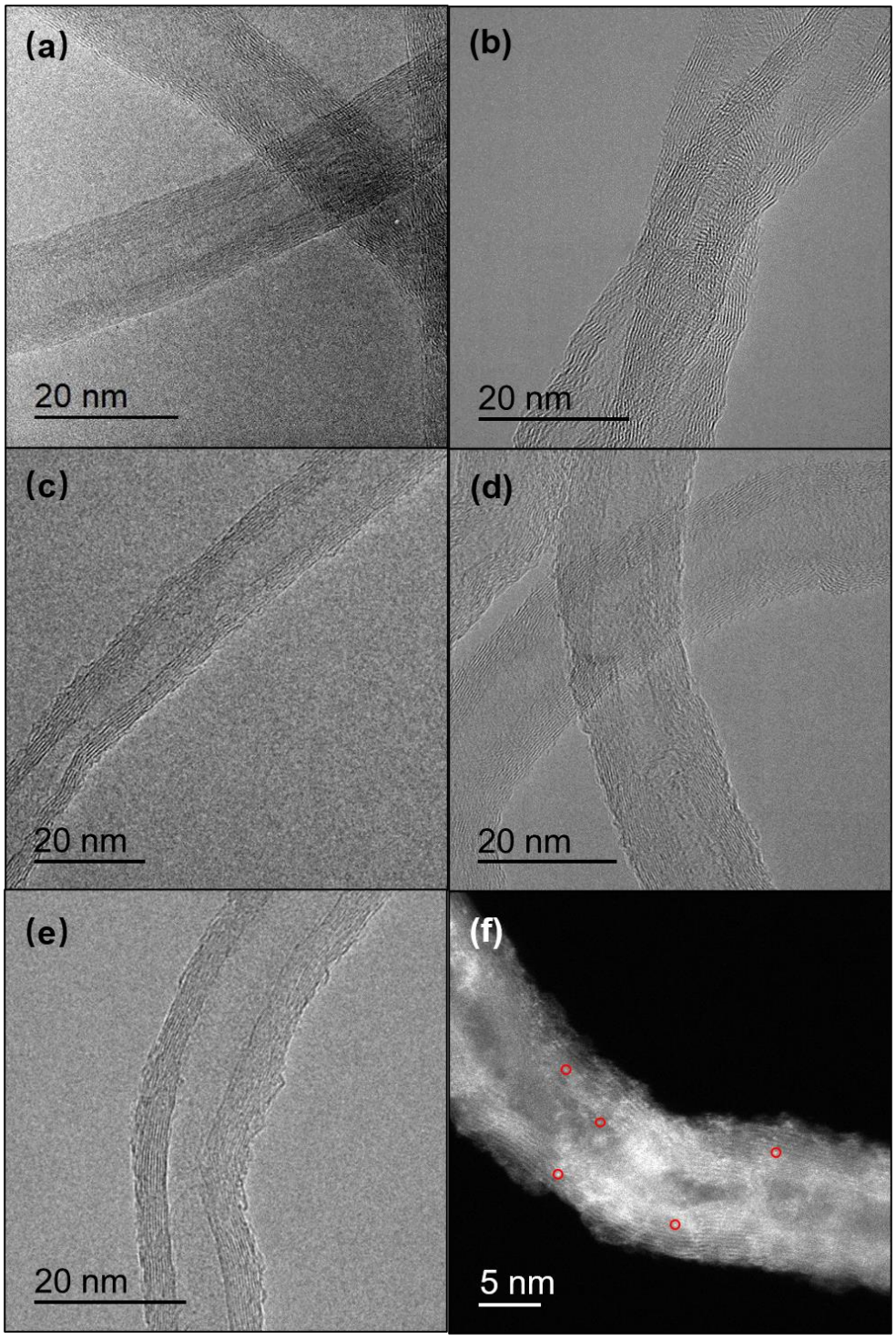

Figure S3. TEM images of (a) CoPc MDE, (b) ZnPc MDE, (c) NiPc MDE, (d) CuPc MDE and (e) MnPc MDE. (f) Aberration-corrected HAADF-STEM image of CoPc MDE and bright dots marked by red circles represent dispersed metal centers in molecules.

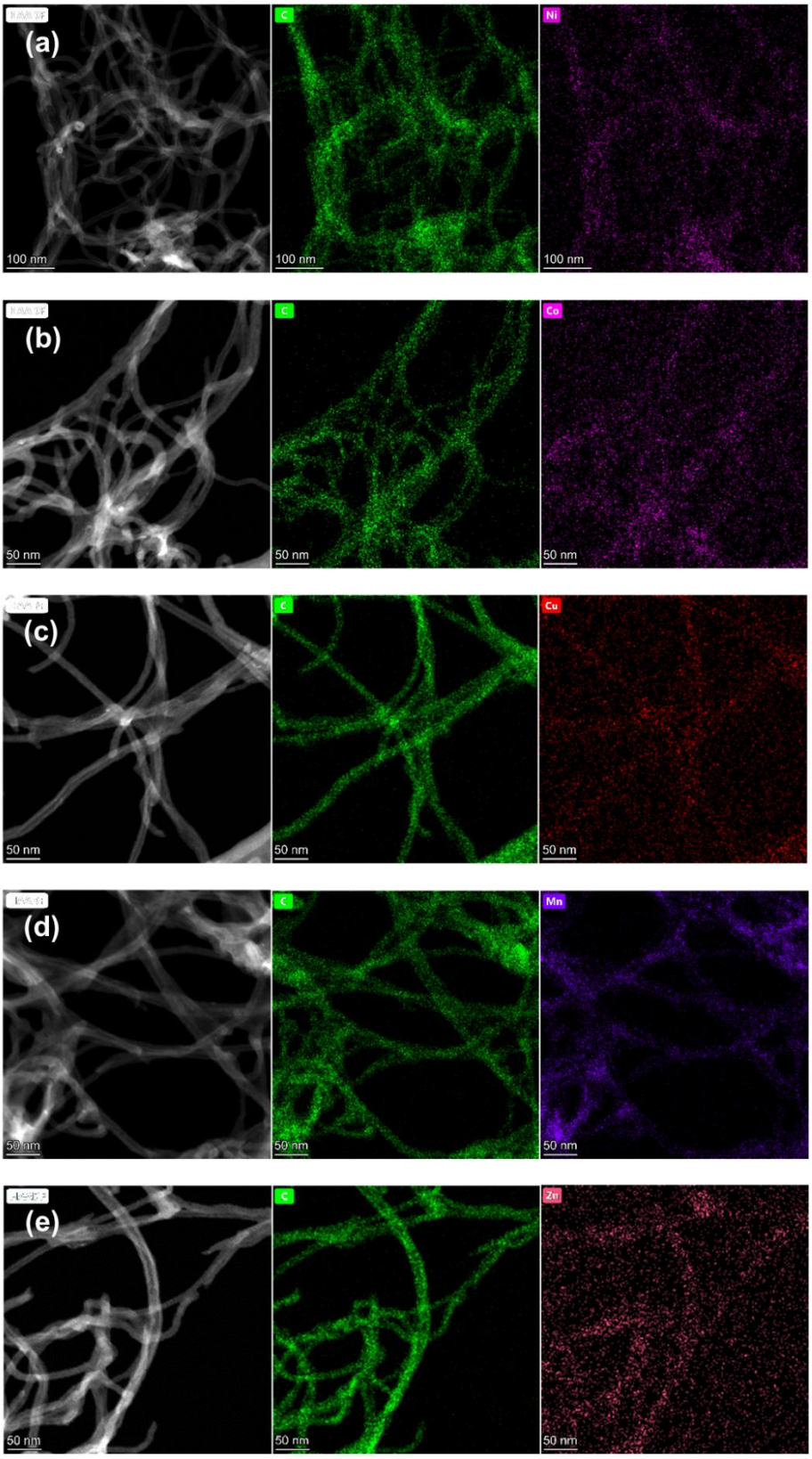

Figure S4. TEM images and EDS elemental mapping images of C and metal of (a) NiPc MDE, (b) CoPc MDE, (c) CuPc MDE, (d) MnPc MDE, and (e) ZnPc MDE.

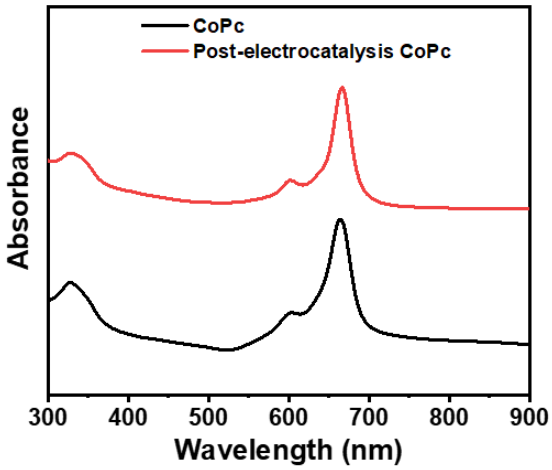

Figure S5. UV-Vis spectra of fresh CoPc and post-electrolysis CoPc in DMF.

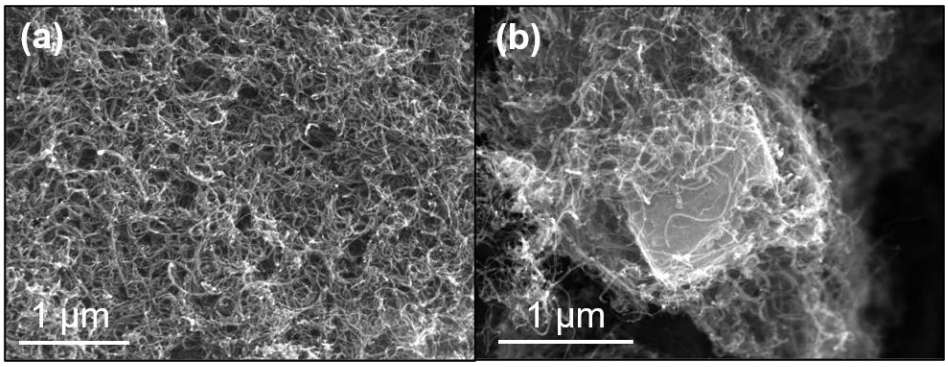

Figure S6. SEM images of (a) CoPc MDE and (b) CoPc+CNT.

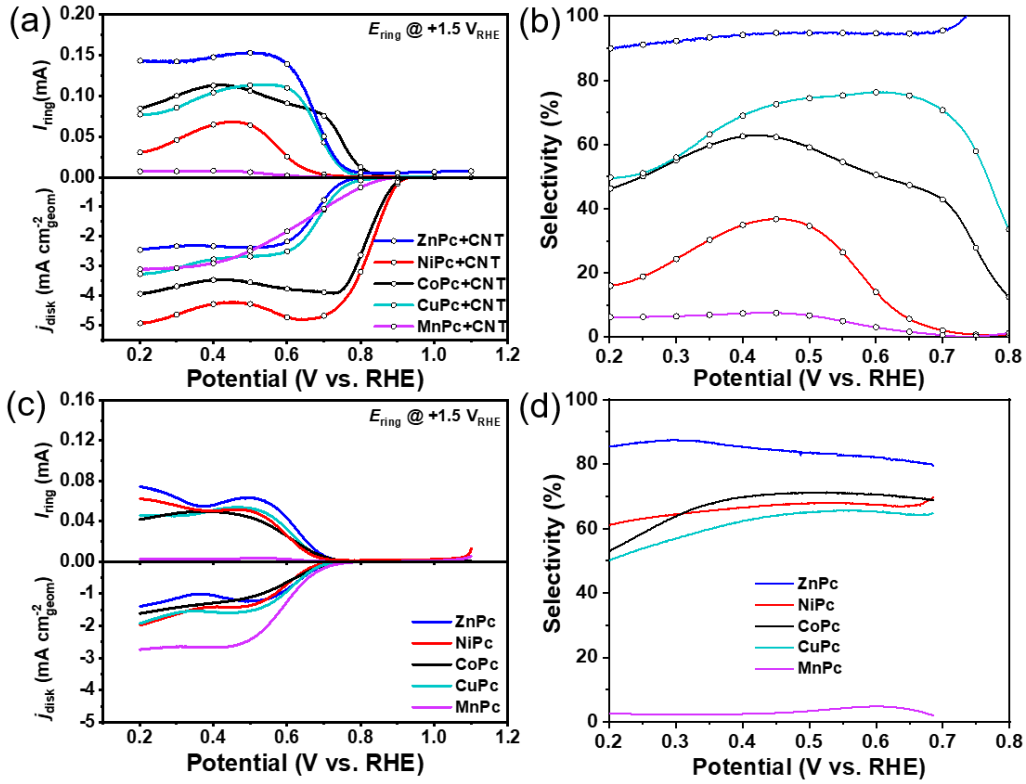

Figure S7. ORR polarization plots for (a) MPc+CNT (M = Zn, Ni, Co, Cu, Mn) and (c) aggregated MPcs with the loading of 0.2 mg cm^{-2} on RRDEs at 1600 rpm in 0.1 M KOH saturated with O_2. Corresponding selectivities of (b) MPc+CNT and (d) aggregated MPcs calculated from RRDE measurements.

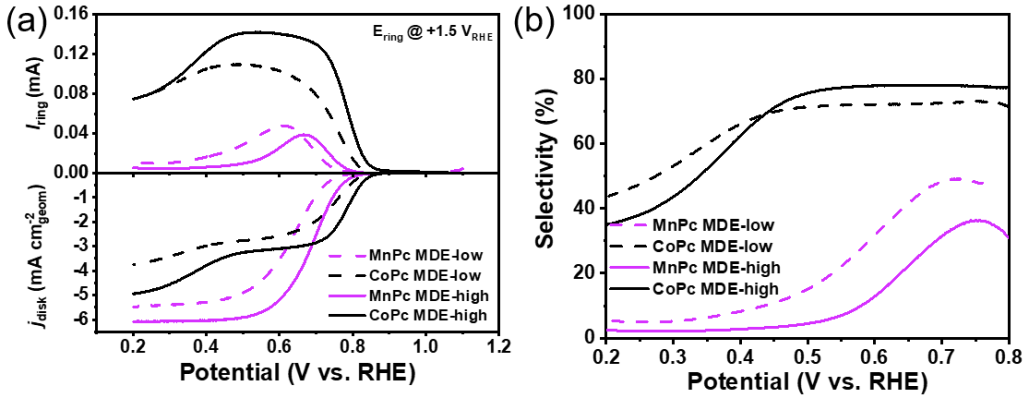

Figure S8. (a) ORR polarization plots for CoPc and MnPc MDEs with the loading of 0.05 (low) and 0.2 (high) mg cm^{-2} on RRDEs at 1600 rpm in 0.1 M KOH saturated with O_2. (b) Corresponding selectivities of CoPc and MnPc MDEs.

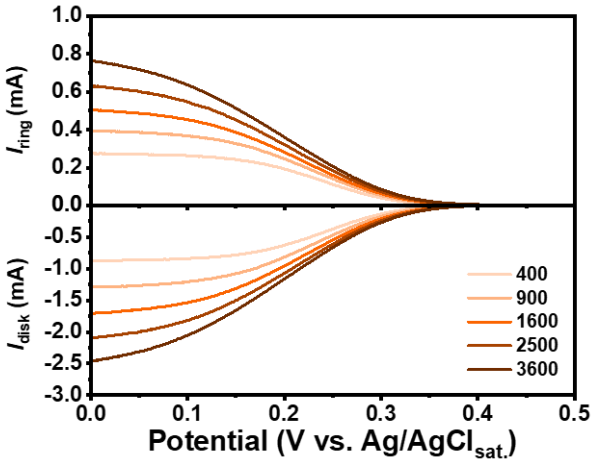

Figure S9. Calibration of the collection efficiency of the RRDE by the redox of potassium ferricyanide.

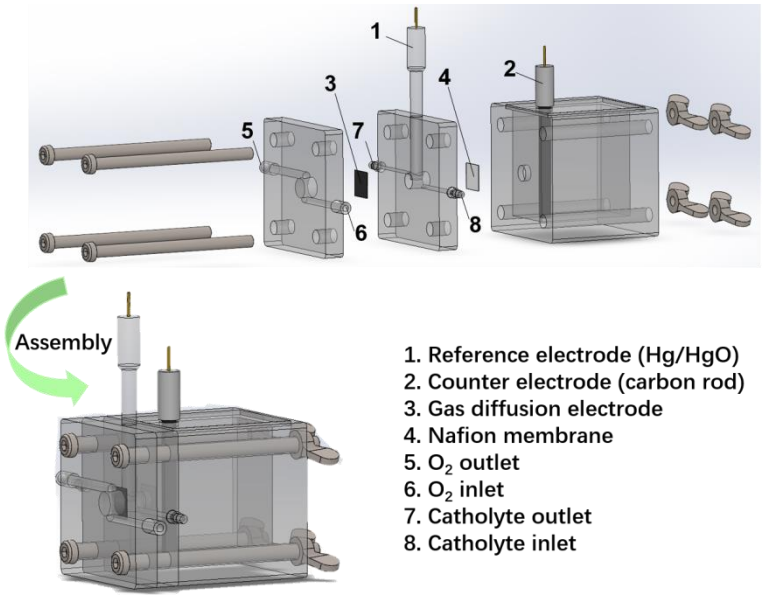

Figure S10. Schematic illustration of GDE.

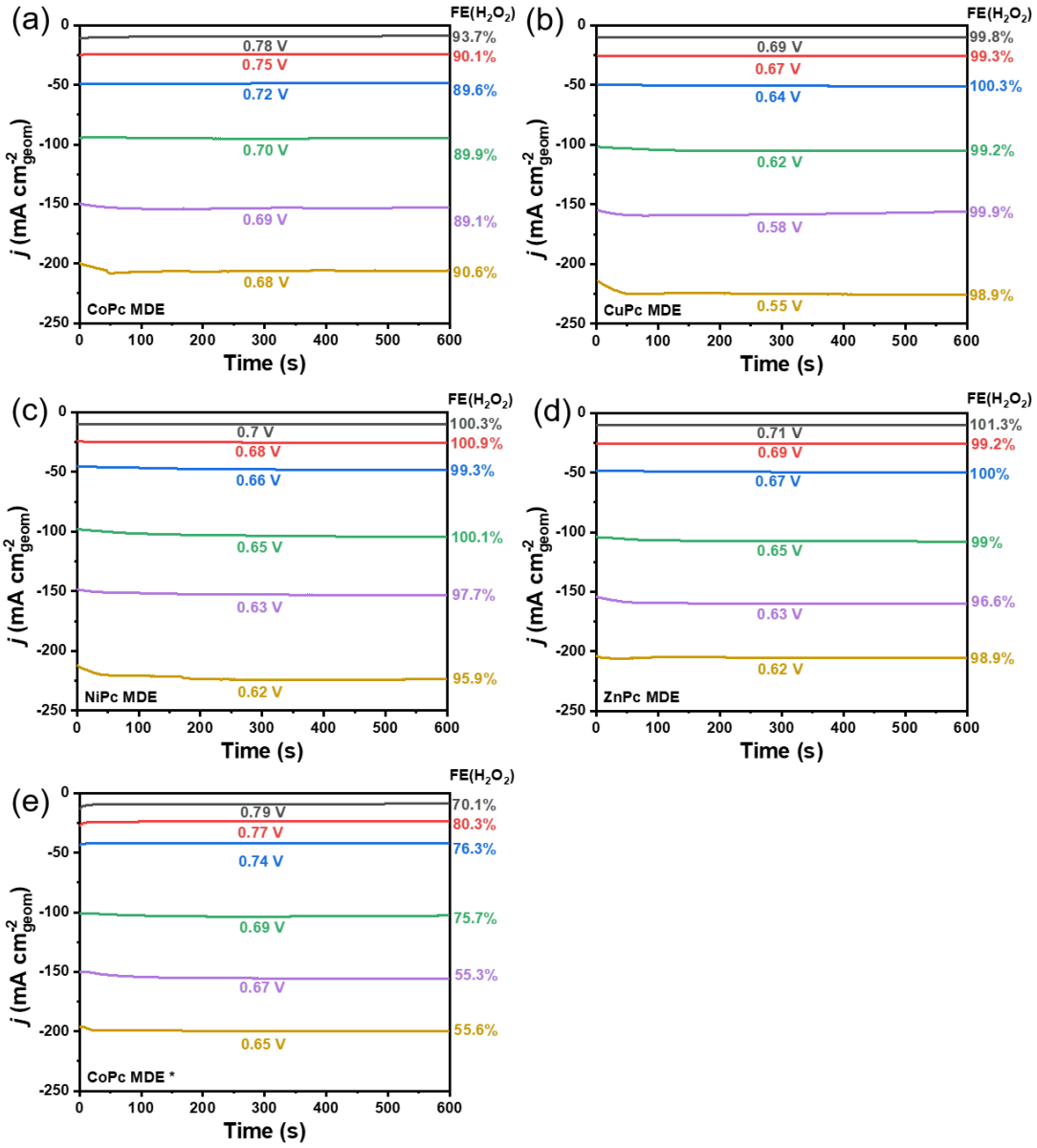

Figure S11. Chronoamperometry of (a) CoPc MDE, (b) CuPc MDE, (c) NiPc MDE, (d) ZnPc MDE with PTFE, and (e) CoPc MDE* without PTFE in GDEs.

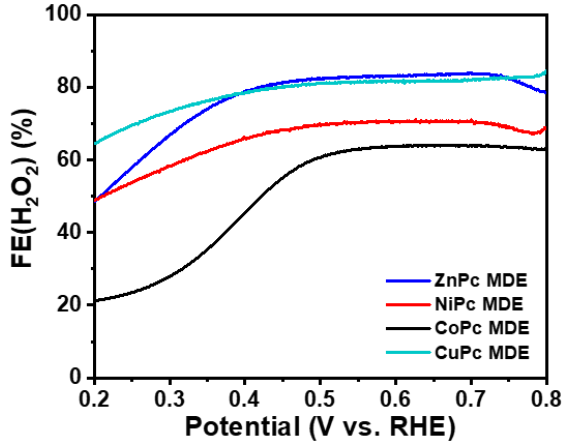

Figure S12. FE(H_2O_2)s of MPc MDEs (M = Co, Ni, Zn, Cu) derived from the selectivities measured by RRDEs.

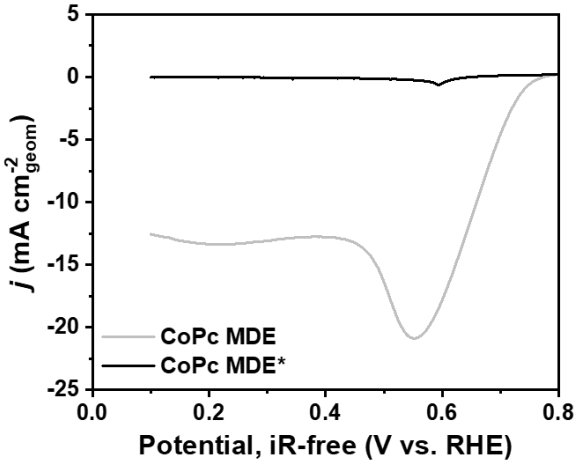

Figure S13. Linear sweep voltammetry of CoPc MDE with PTFE and CoPc MDE* without PTFE tested in a GDE with Ar saturated 1 M KOH (containing 10 mM H_2O_2).

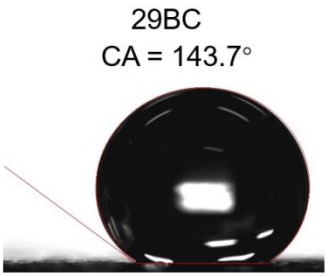

Figure S14. Contact angle of the micro-porous layer of 29BC.

Supporting Tables

Table S1. Free energy of *OOH, *O, *OH, and *H_2O_2 on the metal centers of MPcs in bulk water ($\varepsilon_r = 78.4$) at 0.7 V.

Model	**ZnPc**	**NiPc**	**CoPc**	**CuPc**	**MnPc**
$\Delta G_{*\mathrm{OOH}}$ **(eV)**	2.58	2.64	1.80	2.70	1.47
$\Delta G_{*\mathrm{O}}$ **(eV)**	2.92	2.79	1.36	3.53	-0.10
$\Delta G_{*\mathrm{OH}}$ **(eV)**	0.93	1.28	0.33	1.55	-0.21
$\Delta G_{*\mathrm{H_2O_2}}$ **(eV)**	2.13	2.34	1.98	2.20	2.01

Table S2. Metal contents of MPc MDEs determined from ICP-MS.

Catalysts	ZnPc MDE	NiPc MDE	CoPc MDE	CuPc MDE	MnPc MDE
Metal contents (wt%)	0.59	0.65	0.65	0.59	0.63

Table S3. Electronic energy of *O_2 and *H_2O_2 on the metal centers of MPcs.

Model	**ZnPc**	**NiPc**	**CoPc**	**CuPc**	**MnPc**
$E_{*\mathrm{O_2}}$ **(eV)**	-0.11	-0.11	-0.74	-0.07	-0.77
$E_{*\mathrm{H_2O_2}}$ **(eV)**	-0.16	0.04	-0.26	-0.01	-0.23

Table S4. Free energy of two descriptors of CoPc in bulk water ($\varepsilon_r = 78.4$) and in hydrophobic environment ($\varepsilon_r = 2, 5$) at 0.7 V.

$\boldsymbol{\varepsilon_r}$	**78.4**	**5**	**2**
$\Delta G_{*\mathrm{H_2O_2}}$ **(eV)**	1.97	2.18	2.26
$\Delta G_{*\mathrm{O}} - \Delta G_{*\mathrm{OOH}}$ **(eV)**	-0.44	-0.48	-0.49

Table S5. Catalytic performance of CoPc and ZnPc MDEs in comparison with previously reported electrocatalysts for H_2O_2 production.

Catalyst	Classification	Electrolyte	Potential (V vs RHE)	Reduction current density (mA cm^{-2})	FE(H_2O_2)	Measured time (h)	H_2O_2 production rate (mmol g_{cat}^{-1} h^{-1})	Ref.
CoPc MDE	Metal complex	1 M KOH	0.7 (*iR*)	100	88%	12	8200	This work
ZnPc MDE	Metal complex	1 M KOH	0.65 (*iR*)	100	94%	10	9100	This work
CoTPP/VGCF	Metal complex	PEM	/	90	42%	8	350	15
COF-366-Co	Metal SAC	0.1 M KOH	~-0.3	22	79%	3	909	14
Co-N-C	Metal SAC	0.1 M KOH	/	50	~50%	6	4330	16
Co_1-NG(O)	Metal SAC	0.1 M KOH	0.58 (*iR*)	50	~45%	10	418	17
Co-POC-O	Metal SAC	0.1 M KOH	/	10	64.1%	1.5	478	19
CoNOC	Metal SAC	0.1 M $HClO_4$	0.1	~2.5	95%	11	590	20
Co-N_5	Metal SAC	0.5 M NaCl	/	50	95.6%	24	4500	21
Ni-N_2O_2/C	Metal SAC	0.1 M KOH	~0.38	70	91%	8	5900	22
$Pd^{\delta+}$-OCNT	Precious metal	0.1 M $HClO_4$	0.1	10	87%	~0.6	1700	23
GNP	Carbon material	0.1 M KOH	0.65	~0.5	95%	30	11.4	24
HPC-H24	Carbon material	0.05 M H_2SO_4 + 0.05 M Na_2SO_4	0	/	91.2%	2.5	294	25

PEM means proton exchange membrane was used instead of liquid electrolytes.
SAC means single-atom catalysts.

Supporting References

1. X. Zhang, Z. Wu, X. Zhang, L. Li, Y. Li, H. Xu, X. Li, X. Yu, Z. Zhang, Y. Liang and H. Wang, *Nat. Commun.*, 2017, **8**, 14675.
2. X. Zhang, Y. Wang, M. Gu, M. Wang, Z. Zhang, W. Pan, Z. Jiang, H. Zheng, M. Lucero, H. Wang, G. E. Sterbinsky, Q. Ma, Y.-G. Wang, Z. Feng, J. Li, H. Dai and Y. Liang, *Nat. Energy*, 2020, **5**, 684-692.
3. C. Xia, J. Y. Kim and H. T. Wang, *Nat. Catal.*, 2020, **3**, 605-607.
4. G. Kresse and J. Furthmüller, *Phys. Rev. B*, 1996, **54**, 11169-11186.
5. J. P. Perdew, K. Burke and M. Ernzerhof, *Phys. Rev. Lett.*, 1996, **77**, 3865-3868.
6. J. P. Perdew, M. Ernzerhof and K. Burke, *J. Chem. Phys.*, 1996, **105**, 9982-9985.
7. G. Kresse and D. Joubert, *Phys. Rev. B*, 1999, **59**, 1758-1775.
8. S. Grimme, J. Antony, S. Ehrlich and H. Krieg, *J. Chem. Phys.*, 2010, **132**, 154104.
9. J. K. Nørskov, J. Rossmeisl, A. Logadottir, L. Lindqvist, J. R. Kitchin, T. Bligaard and H. Jónsson, *J. Phys. Chem. B*, 2004, **108**, 17886-17892.
10. V. Wang, N. Xu, J.-C. Liu, G. Tang and W.-T. Geng, *Comput. Phys. Commun.*, 2021, **267**, 108033.
11. K. Mathew, R. Sundararaman, K. Letchworth-Weaver, T. A. Arias and R. G. Hennig, *J. Chem. Phys.*, 2014, **140**, 084016.
12. K. Mathew, V. S. C. Kolluru, S. Mula, S. N. Steinmann and R. G. Hennig, *J. Chem. Phys.*, 2019, **151**, 8.
13. K. Takeyasu, M. Furukawa, Y. Shimoyama, S. K. Singh and J. Nakamura, *Angew. Chem., Int. Ed.*, 2021, **60**, 5121-5124.
14. C. Liu, H. Li, F. Liu, J. Chen, Z. Yu, Z. Yuan, C. Wang, H. Zheng, G. Henkelman, L. Wei and Y. Chen, *J. Am. Chem. Soc.*, 2020, **142**, 21861-21871.
15. T. Murayama, S. Tazawa, S. Takenaka and I. Yamanaka, *Catal. Today*, 2011, **164**, 163-168.
16. Y. Y. Sun, L. Silvioli, N. R. Sahraie, W. Ju, J. K. Li, A. Zitolo, S. Li, A. Bagger, L. Arnarson, X. L. Wang, T. Moeller, D. Bernsmeier, J. Rossmeisl, F. Jaouen and P. Strasser, *J. Am. Chem. Soc.*, 2019, **141**, 12372-12381.
17. E. Jung, H. Shin, B.-H. Lee, V. Efremov, S. Lee, H. S. Lee, J. Kim, W. Hooch Antink, S. Park, K.-S. Lee, S.-P. Cho, J. S. Yoo, Y.-E. Sung and T. Hyeon, *Nat. Mater.*, 2020, **19**, 436-442.
18. J. J. Gao, H. B. Yang, X. Huang, S. F. Hung, W. Z. Cai, C. M. Jia, S. Miao, H. M. Chen, X. F. Yang, Y. Q. Huang, T. Zhang and B. Liu, *Chem*, 2020, **6**, 658-674.
19. B.-Q. Li, C.-X. Zhao, J.-N. Liu and Q. Zhang, *Adv. Mater.*, 2019, **31**, 1808173.
20. C. Tang, L. Chen, H. Li, L. Li, Y. Jiao, Y. Zheng, H. Xu, K. Davey and S.-Z. Qiao, *J. Am. Chem. Soc.*, 2021, **143**, 7819-7827.
21 Q. Zhao, Y. Wang, W.-H. Lai, F. Xiao, Y. Lyu, C. Liao and M. Shao, *Energy Environ. Sci*., 2021, **14**, 5444-5456.
22. Y. L. Wang, R. Shi, L. Shang, G. I. N. Waterhouse, J. Q. Zhao, Q. H. Zhang, L. Gu and T. R. Zhang, *Angew. Chem., Int. Ed.*, 2020, **59**, 13057-13062.

23. Q. Chang, P. Zhang, A. H. B. Mostaghimi, X. Zhao, S. R. Denny, J. H. Lee, H. Gao, Y. Zhang, H. L. Xin, S. Siahrostami, J. G. Chen and Z. Chen, *Nat. Commun.*, 2020, **11**, 2178.
24. G.-F. Han, F. Li, W. Zou, M. Karamad, J.-P. Jeon, S.-W. Kim, S.-J. Kim, Y. Bu, Z. Fu, Y. Lu, S. Siahrostami and J.-B. Baek, *Nat. Commun.*, 2020, **11**, 2209.
25. Y. Liu, X. Quan, X. Fan, H. Wang and S. Chen, *Angew. Chem., Int. Ed.*, 2015, **54**, 6837-6841.